
Article:
Guan, D. orcid.org/0000-0002-3953-2878, Wynne, B., Junheng, G. et al. (2 more authors) (2019) Basal slip mediated tension twin variant selection in magnesium WE43 alloy. Acta Materialia, 170. pp. 1-14. ISSN 1359-6454

https://doi.org/10.1016/j.actamat.2019.03.018

Basal slip mediated tension twin variant selection in magnesium WE43 alloy

Dikai Guan*, Brad Wynne, Junheng Gao, Yuhe Huang, W. Mark Rainforth*

Department of Materials Science and Engineering, University of Sheffield, Sheffield S1 3JD, UK

*Corresponding authors: dikai.guan@sheffield.ac.uk, m.rainforth@sheffield.ac.uk

Abstract:

Tension twinning nucleation and evolution in Mg WE43 alloy over a large sampling area was investigated using a quasi-in-situ EBSD/SEM method during interrupted compression testing. The results showed tension twins with both high and low macroscopic Schmid factor (MSF) were activated under a compressive stress of 100 MPa with a strain rate of 10^{-1} s^{-1}. Basal slip in most grains dominated at this stress, so nucleation of twin variants required little interaction with non-basal slip, which was different from other studies reporting prismatic slip and/or tension twinning were required to activate some low MSF tension twin variants. The geometric compatibility factor (m') was proved to be an important factor to illustrate tension twin variant selection assisted by basal slip. The analysis indicated m' played a critical role over MSF in tension twin variant selection during twin nucleation stage, and final twin variant types were insensitive with increasing stress but they inherited twin variant types determined at twin nucleation stage. Moreover, which specific grain boundary of a grain with hard orientation for basal slip would nucleate which twin variant could be also validated by m' and largely depended on two factors: (a) high value of m' with 1^{st} or 2^{nd} rank between the tension twinning of nucleated twin variant and basal slip in adjoining grains; and (b) intensive basal slip activity in the neighbouring grains before twin nucleation.

Keywords: Magnesium alloy; Deformation twinning; Schmid Factor; Variant selection; EBSD

1. Introduction

As long as the tension/compression force is not perpendicular/parallel to Mg crystal <0001> axis, the $\{10\bar{1}2\}[\bar{1}011]$ tension twin is easily activated when the grains are positioned in hard orientations for basal slip after deformation due to low critical resolved shear stress (CRSS)[1, 2]. There are 6 tension twin variants [3, 4] and it would be expected that the variant with high macroscopic Schmid factor (MSF) will be activated once the applied stress reaches the CRSS [5]. However, it is common to see a non-Schmid behaviour of tension twin variant selection (e.g., tension twin variants with low MSF were activated instead of the variant with the highest MSF)[6-9]. Therefore, MSF is not the only factor to control the twin variant selection meaning other factors need to gain a complete understanding of tension twin nucleation and growth.

Local internal stress introduced during deformation could resolve shear stress on a twin variant with originally low MSF and facilitate its activation. However, the determination of these complex internal stresses is extremely difficult to quantify either by experiment or computation [7, 9]. Recently, some mechanisms have been proposed to explain this non-Schmid tension twin variant selection behaviour. Jonas et al.[7, 8] reported a local strain accommodation model. The activated twin variants with low MSF required less or no strain accommodation via prismatic slip in an adjacent grain than twin variants with high MSF. The CRSS difference between basal, prismatic and even pyramidal slip can be largely reduced by alloying or increasing working temperature[10, 11]. The prismatic slip activity could be enhanced and accommodate the local strain caused by adjacent potential high MSF twin variants. However, considerable low MSF tension twin variants were still observed when AZ31 was deformed at 400 ˚C[12]. Therefore, the retardation of high MSF twin variants in some grains cannot be fully explained by the lack of prismatic slip activities. On the other hand, Shi et al. [9] reported cross-boundary twins with low MSF required the most or more prismatic slip and/or tension twin accommodation. Mu et al. [8] stated the nucleation of secondary contraction and tertiary tension twin variant can be correlated with strain accommodation model, but nucleation of primary tension twin variants was controlled by MSF. Most of these studies only investigated post-mortem samples after deformation. Thus, it was challenging to identify whether twinning occurs before or after slip in the immediate neighbourhood. In addition, if twin growth happened in the investigated samples and both two ends of a twin reached the grain boundary, it was difficult to identify at which grain boundary the twin nucleated at.

Another proposed mechanism is that twin variant selection bears a strong relation with geometrical compatibility factor (m') describing strain transfer or compatibility[6, 13-18], as described in the following equation[19].

$$m' = \cos(\varphi) * \cos(\kappa)$$

Because m' has been extended to explain both slip and twinning [18-21], κ is the angle between slip directions and/or twinning shear directions, and φ is the angle between slip and/or twinning planes normal directions in two adjacent grains.

The activated twin variant normally has a high value of m'. Deformation twin activation can be due to the relaxation of local strain induced by twinning or slip in neighbour grains. For example, slip assisted twins were reported by [14, 22]. The m' factor was often used to explain the variant selection of paired or connected tension twins, but recently used to validate the variant selection induced by slip[4, 14, 16, 18, 23]. The twin nucleation and the direct evidence of slip-twin and twin-twin interactions along various grain boundaries cannot be investigated dynamically by using post-mortem sample analysis. In addition, most research work was based on investigation of conventional AZ31 or AM30 Mg alloy with a strong texture[4, 7-9, 22, 24], but tension twinning behaviour in another group of rare earth (RE) containing Mg alloys with non-basal texture was not thoroughly investigated[16]. Wang et al. [16] used in-situ observation to investigate tension twin variant selection in binary Mg-RE alloys. They proposed m' was an effective criterion in determining tension twin variant selection especially in grains where twinning was not favoured by the loading stress. However, this conclusion was not based on a statistical analysis and the selected areas could not be representative of the global textures [16]. Therefore, further systematic studies of this dynamic twin response behaviour in Mg-RE systems needs to be conducted.

Furthermore, a grain normally has average 6 grain boundaries in a 2D sampling surface. Therefore, combined the 6 twin variants per grain, there would be 36 possibilities of a potential twin variant nucleated at a specific grain boundary in a grain. It is a wide open question that which grain boundary or boundaries would be the preferable nucleation sites for specific tension twin variant(s). Moreover, all aforementioned studies have not studied whether tension twin variant selection is determined at the nucleation stage at low loading stress or is sensitive to the increasing stress, since non-basal slip normally occurs at high stress, which might change the twinning behaviour induced mainly by basal slip at low stress.

To address these critical issues described above and find a general tension twin variant selection criteria at grain boundary level in Mg-RE alloy, this study employed a quasi-in-situ EBSD/SEM method to track the interaction between twin and twin/slip through

the entire compression tests using a WE43 alloy sample. Tension twins with both low and high MSF appeared when the sample was compressed to a stress of 100 MPa. Besides tension twins, only basal slip was activated in most grains, minimising the influence of other slip systems on twin variant selection. The results indicate the activated twin variants normally have 1^{st} or 2^{nd} rank of m', but the MSFs rank from 1^{st} to 4^{th}. In other words, the m' factor is more relevant than MSF to determine tension twin variant selection in the present case. Moreover, tension twin variant types were insensitive to increasing stress but they were inherited twin variant types determined at twin nucleation stage. These results can enable us to accurately predict the twinning behaviour including not only of variant selection but also nucleation position in Mg alloys.

2. Experimental

2.1 Material

A commercial WE43 alloy supplied by Magnesium Elektron in as-extruded T5 bar form was used in this work. Several rectangular slabs 5(RD)×5(RD) ×10(ED) mm^3 was cut by electrical discharge machining from the extruded bar (where RD is radial direction, ED is the extrusion direction). Solid solution treatment was carried out in a tube furnace with continuous argon flow at 525 °C for 1 hour, followed by cold water quenching[25].

2.2 Sample preparation for quasi-in-situ EBSD of compression test

The heat treated samples were ground and polished using SiC paper, 1 μm, 0.25 μm oil-based diamond suspension, 40 nm OPS suspension. After EBSD scanning, the sample was compressed up to a compressive stress of 100 MPa using a Zwick/Roell universal testing machine at a strain rate of 10^{-1} s^{-1} along one RD direction. The load was then removed immediately and the sample was quickly transferred using a vacuum container to the SEM chamber for further EBSD scanning of the same area that had been scanned before compression. This cycle of compression and EBSD scanning was repeated on the same sample at compressive stresses of 150 MPa, 250 MPa, and 300 MPa. The detailed slip traces and twin distribution within the same sampling area after each compression test were analysed by using Matlab with MTEX codes [26]. Values of the m′ factor were calculated using in-house codes.

All the EBSD data were collected from the centre of surface plane RD-ED in this study. All Euler EBSD images were used in this work because commonly used Inverse Pole

Figure (IPF) images cannot clearly distinguish crystal orientations with similar Z axis. The compression test loading direction, EBSD map and pole figure colour legend and coordinate system were all the same as presented in Fig. 2 throughout this paper.

3. Results

3.1 Compression curves

Preliminary work showed that the yield strength of this heat-treated WE43 alloy was around 150 MPa. Therefore, the interrupted compression stresses chosen in this study were 100, 150, 250 and 300 MPa in order to fully capture the twin nucleation and subsequent evolution.. Fig. 1 shows the corresponding compression curves interrupted at the four stresses. It was evident that this sample started to yield around 150 MPa with a strain rate of 10^{-1} s^{-1} and so 100 MPa was prior to yielding and all other stresses were post-yield.

3.2 Initial microstructure

Fig. 2(a) shows the EBSD all Euler map of the sample before compression. This sampling area consisted of 443 grains. Some undissolved second phase particles were sparsely distributed in some grains, but most grain boundaries were clear of second phase particles, as shown in Fig. 2(b). Fig. 2(c) clearly indicates that this sample does not have a strong basal texture compared to other published work on AZ and AM Mg alloys[4, 7, 9, 14, 22, 24]. This micro-texture determined by EBSD was very similar to the micro-texture of other samples from different parts of the same bulk sample, as shown in Fig. 3. It should be noted that although the EBSD mapped area in Fig. 3(b) was nearly four times larger than Fig. 2(a), their micro-textures were nearly the same, in terms of texture intensity and texture component distribution. Therefore, this micro-texture of sample used for quasi-in-situ EBSD/SEM in Fig. 2 was representative of the global texture of the large bulk sample.

3.3 Twin nucleation and growth

Fig. 4 presents a typical SEM image of a large area after compression at the stress of 100 MPa and corresponding predicted basal slip trace distribution. Most slip traces existed in the polished sample surface after stress at 100 MPa matched very well with the predicted basal slip traces in grains with high basal slip MSF. It should be noted twinning and some very limited non-basal slip occurred in grains A, B, C, D and E due to a low MSF for basal slip in these grains. Agnew et al. [27] reported the CRSS of deformation modes in the same solutionised WE43 alloy with similar average grain size (e.g., basal slip: 12 MPa, tension

twinning: 85 MPa, prismatic slip: 78 MPa and pyramidal <c+a> slip: 130 MPa). At the compressive stress of 100 MPa, the macro maximum resolved sheared stress cannot exceed 50 MPa with largest MSF 0.5 for all deformation modes. The activation of basal slip can be attributed to macro stress, but the tension twin nucleation cannot be attributed to macro stress since 50 MPa is much lower than the tension twinning CRSS of 85 MPa. Therefore, the nucleated tension twins even with the highest MSF could be only activated with the assistance of local internal stress. For instance, the accumulated internal stress can be induced by intensive basal slip. Additionally, only isolated non-basal slip was observed and therefore the effect of non-basal slip on tension twin nucleation can be ignored.

Fig. 4(a) clearly shows intensive basal slip occurred adjacent to poorly developed twins (e.g., twins in grains A, B, C, E). This suggests basal slip occurred before the activation of twins. To further validate this, Fig. 5 provides two representative areas during interrupted compression testing. In these two sets of images, no twin nucleation occurred when the stress was 100 MPa, but intense basal slip in the adjoining grains was activated, Fig. 5(a) and Fig. 5(d). With increasing stress, twins were gradually nucleated and developed at the grain boundaries where intensive basal slip intersected the boundary. Therefore, the reported CRSS [27] and these representative images confirmed basal slip assisted tension twin nucleation. In references [7, 8], the strain accommodation model was established on the hypothesis: if twinning occurred, the slip and/or tension twinning in neighbouring grains ensued to accommodate the strain induced by twinning. Evidently, Fig. 4 and Fig. 5 showed the opposite: tension twinning was activated to accommodate the strain induced by intensive basal slip in adjoining grains. This could also be categorised as strain accommodation, but the subject and object were replaced.

It is desirable to analyse the twin nucleation under compressive stress of 100 MPa since only basal slip was significantly activated while other non-basal slip activities were very limited. In the following sections, 4 representative regions of interest in this sample (areas marked in Fig. 2(a)) were chosen to illustrate the tension twinning behaviour systematically.

3.3.1 Tension twin variant nucleated with the 1st highest MSF (m)

Fig. 6(a) and Fig. 6(b) give an EBSD band contrast map and corresponding SEM image of the region of interest 1 for the sample compressed to 100 MPa. Several twins were nucleated along grain boundaries between grains 1 and 1-5, and grains 1 and 1-1, despite the applied stress being below the macroscopic yield strength. For $\{10\bar{1}2\}[\bar{1}011]$ tension twin

mode, there are 6 twinning variants that can be activated [3, 4]. When a twin is activated, the parent grain and twin share one plane which is referred to as the twinning plane. When illustrated on a pole figure, the position of the shared plane is normal to the orientation of the twin trace[28, 29]. This method was used to identify which specific twin variant was activated in grains in this study. Fig. 6(c) provides a $(10\bar{1}2)$ pole figure of grain 1. It clearly illustrates the position of 6 potential tension twin variant position, and the tension twin variant with the highest m of 0.452 was activated in grain 1.

Fig. 6(d) and Fig. 6(e) show band contrast and All Euler EBSD maps of the region of interest 1 after being compressed to a maximum stress of 150 MPa. As shown in the SEM image of grain 1 in Fig. 6(g), only basal slip occurred in slip activated neighbouring grains. Twin growth took place but no new twin variant was produced when the stress was increased to 150 MPa. Fig. 6(f) provides a basal MSF distribution superimposed with the predicted basal slip traces (grey dash lines shown in Fig. 6(f)). The predicted slip traces matched well with the existed slip traces in Fig. 6(b) and Fig. 6(g). After completely examining the EBSD band contrast image of the entire sampled area, the accommodated strain was not clearly observed using band contrast image. For example, the band contrast of the areas in grains 1-1 and 1-5 near corresponding adjoining twins was not changed (Fig. 6(a) and Fig. 6(d)). This meant the strain introduced by intensive basal slip was relaxed or accommodated by nucleation tension twins in adjoining neighbour grains. As shown in Figs. 4-6 and the figures in the following sections, basal slip traces were densely distributed in most grains. The twins in grains with low MSF of basal slip were usually nucleated in front of a grain boundary where intensive basal slip occurred on the other side. Therefore, basal slip played an essential role in twin formation.

To confirm this, the m' factor was used to correlate with twin variant nucleation and slip. m' was calculated between basal slip of each neighbouring grain and 6 potential tension twin variants of grain 1, unless the neighbouring grain shows other deformation activities other than basal slip (e.g., tension twin occurred in grain 1-2), as listed in Table 1. The MSF is also given for each tension twin variant in Grain 1. It was observed that the specific tension twin variant preferred to be nucleated at grain boundaries with higher m' and intensive basal slip activity (e.g., grain boundaries between grains 1 and 1-1, and between grains 1 and 1-5). It should be noted one of the twin-twin m' values between grain 1-2 and grain 1 was as high as 0.884, so the corresponding twin variant would be nucleated once the local stress increased.

Tracking the same area after further compression to 250 MPa, a tension twin variant with the highest m' was nucleated and marked by a red arrow in Fig. 6(h), which was

consistent with the reported twin-assisted arguments[4, 22]. Although m' between grain 1-6 and grain 1 was 0.741 and basal slip MSF of grain 1-6 was 0.37, basal slip activity was not intensive at the grain boundary. This may be attributed to the kink produced in front of the slip traces due to local shear. Since there was no basal slip activity and twinning activity in grain 1-4, no transmission activity needed to be considered. Additionally, two sets of prismatic slip activities were induced by the tension twin and basal slip in grains 1-2 and 1-3 when the applied stress was 250 MPa.

Tracking the same area after further compression to 300 MPa, it was evident that the twin grew with the increased stress. The new twins produced at higher stress had the same variant type as the pre-existing twins formed at the lower stress, with no new tension twin variants produced.

Grain 1-2 had a relatively high basal slip MSF of 0.38, but basal slip was not activated during the entire compression process. In contrast, the tension twin variant with a MSF of 0.31 was preferentially activated. Again, this can be linked to m'. The grain on the left hand side of grain 1-2 exhibited intensive basal slip. The accumulated dislocations around the grain boundary could result in strain in the adjoining grain by either twinning or slip. The m' values of basal slip-tension twin and basal slip-basal slip between grain 1-2 and the corresponding left grain were 0.884 and 0.376, so tension twins were favourably produced.

3.3.2 Two tension twin variants activated in the same grain

Fig. 7(a) shows the region of interest 2 after being compressed to 100 MPa. Two sets of twins were identified in the all Euler map of Fig. 7(a), which shows that these two sets of twins seemed to belong to the same twin variant. However, the corresponding SEM image shown in Fig. 7(b) clearly indicates these two sets of twins with different contrasts had different orientations. Fig. 7(c) shows these two tension twin variants were opposite to each other in the pole figure and their misorientation was nearly 180° rotated along the sample surface normal, so the Kikuchi bands of these two orientation are very difficult to be distinguished by EBSD resulting in artefacts in some cases. This can be further validated when the sample was further compressed up to 150 MPa and 250 MPa and will be discussed in the following context.

Table 2 lists the m' between basal slip of nine neighbouring grains and 6 potential tension twin variants in Grain 2, tabulated with the MSF for each twin variant. The tension twin variants with MSF of 0.498 and 0.489 both had high m but the grain boundaries at which nucleation occurred were quite different. The reason for this was the m' factor between

basal slip in grain 2-1 and the 2nd highest m twin variant in grain 2 was much higher than the 1st highest m twin variant. The former was 0.888, but the latter was only 0.073. However, the m' factor between grains 2-2 and 2 showed the opposite, so the highest m twin variant was preferred nucleated along this grain boundary. For other neighbouring grains, there were either limited basal slip activity in the neighbouring grains or low m', so no twin was nucleated along other grain boundaries. It should be noted at the upper-left corner of grain 2, some twins were found around grains 2-4 and 2-5. The occurrence of these twins was related to the local stress of the kink caused by pyramidal slip, and this is not the main focus of this paper but will be discussed in another paper.

Fig. 8 shows the twin growth behaviour in grain 2 after being compressed to 150 MPa and 250 MPa. More twins were produced due to increased compressive stress, but again no new twin variant was activated, Fig. 8(a-b). In Fig. 8(c-d), the exact orientation of the twin variant with m of 0.498 was still mis-indexed as a twin variant with m of 0.489, since these two variants have very similar EBSD Kikuchi patterns in this case as mentioned above. However, a small part of the former twin variant was correctly indexed in Fig. 8(c). This became clearer in Fig. 8(d) with stress up to 250 MPa.

3.3.3 Tension twin variant with a small macroscopic Schmid factor activated favourably in a grain

Fig. 9(a) shows the region of interest 3 in Fig. 2(a) after being compressed to a stress of 100 MPa. Fig. 9(a) gives the EBSD all Euler map which only shows traces of one twin variant, although three twin variants can be identified in the corresponding SEM image (Fig. 9(b)). The EBSD failed to index all twins because of their small size. Fig. 9(c) clearly identified each twin variant position and matched well with the twinning plane traces in Fig. 9(a-b). Surprisingly, the twin variant with the 4th highest m was preferentially nucleated at the grain boundary. Table 3 lists the m' between basal slip of five neighbouring grains and 6 potential tension twin variants in Grain 3. The m' between basal slip of grain 3-2 and the tension twin variant with 4th highest MSF was the highest at 0.816. The other two twin variants were nucleated along grain boundary between grains 3-3 and 3 with high values m' of 0.867 and 0.843. Other twin variants were not nucleated along grain boundaries due to either limited basal slip activity or low m'.

Fig. 10(a-b) gives the SEM images of Grain 3 after being compressed at 150 MPa and 250 MPa, and Fig. 10(c-d) provides the corresponding all Euler EBSD images. Because grain 3-5 had a basal slip MSF of 0.33 and the m' between basal slip of grain 3-5 and the highest m

tension twin variant of grain 3 was 0.712, the tension twin should be nucleated at the shared grain boundary. The reason for this is again due to the absence of basal slip activity at 100 MPa. When the stress was increased to 150 MPa, the basal slip was activated in grain 3-5 and tension twin occurred subsequently in grain 3 (red arrow shown in Fig. 10(a)). With increasing stress to 250 MPa, more twins were stimulated by basal slip, but again no new twin variant was nucleated.

3.3.4 Tension twin variant with the 2nd highest m activated in a grain

Fig. 11(a) gives the region of interest 4 in Fig. 2(a) after being compressed to a stress of 100 MPa. In Fig. 11(b), the EBSD All Euler map only shows one twin variant due to indexing problems associated with the small twin size. However, the SEM image shown in Fig. 11(b) clearly shows a set of twins having the same variant type were activated at the grain boundary between grains 4-1 and 4. Fig. 11(c) shows that the activated twin variant was the one with the 2nd highest m. Table 4 lists m' between basal slip of five neighbouring grains and 6 potential tension twin variants in Grain 4. The m' between basal slip of grain 4-1 and the 2nd highest m tension twin variant was the highest of 0.987. The twin variant with the highest m of 0.440 was not nucleated at any grain boundaries of grain 4 due to either low m' or limited basal slip activity in neighbour grains. Additionally, a twin can be identified in grain 4-5 and this was caused by the twin transmission from grain 4 to grain 4-5 due to high m' of twin-twin transmission. This has been already mentioned in Fig. 6(h) and will not be stated again in this case.

3.4 MSF(m)-m' ranks

To obtain a statistical result, all the nucleated tension twins in the entire big sampling area after being compressed at 100 and 250 MPa in Fig. 2 were analysed by the same way as illustrated in sections 3.1-3.4. Fig. 12 (a-c) shows some tension twins were activated around kink bands, bugling grain boundaries or were isolated in the grain interior without connecting any grain boundaries (marked by red arrows in Fig. 12). These twinned grains (about 2% of total twinned grains) were excluded for statistical analysis of MSF(m)-m' ranks, since they were more likely to be caused by local stress fluctuation and/or strain transmission from the grains below the sapmpling area surface. After ignoring these small amount of twinned grains, the number of other tension twins, nulceated at grain boundaries in 47 grains, was 237 after sample being compressed at the stress of 100 MPa. At the stress of 250 MPa, the number of

twinned grains was 55 with 345 tension twins. These tension twins were considered for statistical analysis below.

Fig. 13(a) presents the MSF(m)-m' ranks after the sample was unloaded at 100 MPa. Regarding m', it is evident that nearly all the tension twin variants had the 1st or 2nd ranks of m'. However, only 73.3% of the tension twin variants had the 1st and 2nd ranks of MSF. Low MSF tension twin variants accounted for a considerable amount (e.g., 26.6%) of total tension twins. Moreover, it was obvious that the fraction of tension twin variants with 1st rank of m' (80.5%) was around 2 times of variants with 1st rank of MSF (38.6%). This clearly indicated m' played a more critical role than MSF in tension twin variant selection during twin nucleation stage. When the sample was compressed at 250 MPa, most new activated twins were continuely produced in the existed twinned grains appeared at the stress of 100 MPa. These twins normally inherited the same twin variant types. In addition, approximately 8% twins from new twinned grains were produced with various MSF were further activated at the stress of 250 MP, but all these twins still had the 1st or 2nd m' rank. Fig. 13(b) shows all produced twin variants after being compressed up to 250 MPa. The fractions of twin variants with 1st m' and MSF were both increased, but the fraction of tension twin variants with 1st rank of m' (82.9%) was still significant higher than twin variants with 1st rank of MSF (45.5%). Overall, the fraction distribution of twin variant MSF and m' ranks at the stress of 250 MPa was quite similar to the twin variant nucleation at the stress of 100 MPa.

Therefore, there was no significant difference in tension twinning behaviour from 100 MPa to 250 MPa, which indicated that twin variant activation was determined at low stress, only 100 MPa in this case. Further increasing compressive stress mainly influenced and assisted twin growth. With increasing stress, non-basal slip activities including prismatic and pyramidal slip systems were increased. However, after careful examination of the entire sampling area, no new twin was directly linked or produced around non-basal slip areas.

3.5 The effect of de-twinning behaviour on twinning behaviour during interrupted compression test

De-twinning occurs significantly when the external force is reversely loaded in Mg alloys[11, 30, 31]. However, de-twinning only slightly happened if only unloading the original force[30]. In this study, the compression test was interrupted at the stress of 100, 150, 250 and 300 MPa. Fig. 13 already proved that the twinning behaviour was quite similar between the stress of 100 and 250 MPa, which indirectly confirmed that the de-twinning effect on variant selection can be dismissed in this work. Otherwise, the twinning behaviour

should be quite different between low and high stresses if the de-twinning effect was significant. Moreover, slip trace tracking using nice polished sample in this work can further confirm this.

Basal slip can be favourably activated in the tension twins if the basal slip MSF in the twins is relatively high. Once basal slip happens in the twins, the basal slip traces appear on the polished surface and do not disappear when the de-twinning happens. Fig. 14 presents a typical de-twinning region. In Fig. 14(a), weak basal slip traces (marked by blue line) of the right grain can be observed due to low MSF of basal slip (Fig. 14(c)) and several tension twins were produced after being compressed at 100 MPa. In contrast, the basal slip traces of the activated twins (marked by green line in Fig. 14(b)) were quite evident because of high MSF of basal slip. It was not difficult to observe that some of the basal slip traces were out of twinning boundaries (marked by red arrows). This was caused by de-twinning or twinning shrink when the external compressive force of 100 MPa was unloaded. When the compressive stress was increased and unloaded at 250 MPa, this de-twinning behaviour was more obvious (Fig. 14(b)). However, this de-twinning behaviour did not affect the twining variant selection: activated twins were only shrunk but not disappeared, and the tension twin variant selection behaviour was quite similar at the stress of 100 and 250 MPa (Fig. 13). Therefore, the effect of de-twinning on tension twin variant selection could be ignored in this study.

4. Discussion

Based on the above experimental results, it is evident that MSF is not the only factor in determining tension twin variant selection, no matter whether this specific variant had a high or low MSF. Otherwise, no twinning should occur at the macro stress of 100 MPa. The strain accommodation model[7-9] requiring slip and/or tension twinning to accommodate strain induced by either compression or tension twinning cannot correlate with twin variant formation in this work, since the twin activation did not result in the basal or prismatic or pyramidal in the neighbouring grains but accommodated the strain induced by basal slip in adjoining grains. Other non-basal slip activities were very limited due to low external macro stress of 100-150 MPa during tension twin nucleation. Therefore, basal slip occurring in the neighbouring grains was the main reason for tension twinning nucleation. Tension twin variant selection in the twined grains can be correlated with m'.

After examining the sample throughout the compression range used, it appeared that intense basal slip occurred before the formation of most twins. Basal slip traces were distributed across paired neighbouring grains during twin nucleation stage (e.g., after being

compressed at 100 MPa). With further compression, the existing twins grew and new twins were produced ahead of intensive basal slip traces or tension twins (Figs. 4-11). This direct evidence indicated that basal slip occurred earlier than twin nucleation and directly assisted twin nucleation in paired neighbouring grains. The m' between basal slip in neighbouring grains and tension twins in twinned grains not only validated the formation of specific twin variants in the centred grains shown in Fig. (6-11), but also can be used predict and determine which grain boundary would nucleate the corresponding twin variants combining the basal slip behaviour in the adjoining grains and m'. Figs. 6-11 presented several pairs of grains with soft-hard orientations for basal slip. Once deformation started by basal slip in most soft grains where basal slip was favoured, the basal dislocations were accumulated at the boundaries shared with hard grains. Therefore, deformation modes including twinning and slip need to be activated in the neighbouring grain to relieve local stress concentration if the dislocation pile-ups can be fully or partly transmitted. This argument can be also extended to explain the preferable selection selection of tension twinning instead of basal slip (e.g., Fig. 6(g)) in some grains and activation of non-basal slip like prismatic slip (e.g., Fig. 6(h)), but further systematical analysis will be required to obtain a solid conclusion.

In tables 1-4 and Fig. 12, all the activated twin variants including high MSF and low MSF can be correlated with intensive basal slip or twinning activities in neighbour grains: nearly all the activated twins after being compressed at 100 MPa and 250 MPa had a 1st or 2nd rank of m', but the tension twin variants with MSF ranks ranged from 3rd to 6th occupied 26.6% and 22.8% after being comparessed at 100 and 250 MPa. This indicated m' played a critical role in controlling tension twin variant selection in this study, while MSF was less important, especially in twin nucleation stage. The statistical results analysis indicated a simple general criteria for tension twin variant selection in WE43 alloy and all the twins fall within one group only instead of 2-4 groups reported in other publications[7-9, 12, 32]. Which tension twin variant will be nucleated in which specific grain boundary largely depended on two factors: (a) high value of m' between the nucleated twin variant and basal slip in neighbouring grains; and (b) intensive basal slip activity in the neighbouring grains before twin nucleation. Certainly, the neighbouring grains above and below the centred grains in all the sampling area were not considered in this work, but a research of 3D analysis of tension twin variant selection is now ongoing.

It is also found the final twin variant types were mostly determined at the very early stage of compression. The subsequent increased stress further increased the twin number and facilitate the twin growth. Increasing stress did not change the tension twinning variant

selaction behaviour considerably. This was confirmed by statistical analysis of slip trace in each grain by using the combination of SEM and EBSD (e.g., Figs. 4-11) and the results were summarised in Fig. 13. The tension twin variants with higher MSF had a growth advantage over the tension twin variants with lower SF within the same deformed grain, which was consistent with the results concluded in [6], but more systematic work will be needed to thoroughly investigate this.

During twin growth, some twins grew across the grain to reach the opposite grain boundary. Whether these twins could be transmitted into the neighbouring grains or were constrained inside the twinned parent grains was correlated with m'. For example, the twin assisted twin variants shown in Fig. 6(h) and Fig. 11(b) both had the highest m' of 0.854 and 0.700, respectively.

5. Conclusions

$\{\mathbf{10\bar{1}2}\}[\mathbf{\bar{1}011}]$ extension twinning nucleation and evolution behaviour were thoroughly and statistically investigated by quasi-in-situ EBSD and SEM during interrupted compression tests of a WE43 alloy sample which represented the global texture of large bulk sample**.** The main conclusions drawn were:

(1) Tension twins with both high and low MSF can be activated under the compressive stress of 100 MPa before reaching CRSS of tension twinning in WE43. Therefore, tension twin variant selection, even twin variants with high MSF, was not controlled by MSF, which was opposite to the conclusion in ref.[8].

(2) Basal slip dominated at the stress of 100 MPa, so the twin variant nucleation required no or significantly less interaction with non-basal slip, especially prismatic slip. This was different with the conclusions listed in ref. [9, 32] reporting prismatic slip was required to activate one group of low MSF tension twin variants.

(3) The twinning shear accommodation model proposed in Ref. [7, 8], which requires slip and/or tension twinning to accommodate strain induced by either compression or tension twinning, cannot correlate with twin variant formation in this work, which reveals that twin activation in one grain often did not result in basal or prismatic slip in its neighbouring grains.

(4) After tracking the same area, the direct evidence showed that twinning normally occurred after intense basal slip in adjacent grains at the stress of 100 MPa. The twinning or other very limited non-basal slip that occurred was induced by intense basal slip in neighbouring grains, due to relaxation of local strain accumulated by basal slip, or slip strain transmission.

(5) Nearly all activated twin variants after being compressed at 100 MPa and 250 MPa had a 1st or 2nd rank of **m'**. However, low MSF tension twin variants occupied a considerable amount (e.g., 26.6% and 22.8% at the stress of 100 and 250 MPa) of total tension twins. The fraction of tension twin variants with 1st rank of m' was much higher than tension twin variants with 1st rank of MSF, which implied that **m'** played a critical role in controlling tension twin variant selection in this study. MSF was less reliable than m' as a predictor of variant selection, especially at low compressive stress.

(6) Which tension twin variant was nucleated at which specific grain boundary could be determined by **m'** and largely depended on two factors: (a) a high value of **m'** between the nucleated twin variant and basal slip in neighbouring grains; (b) intensive basal slip activity in the neighbouring grains before twin nucleation. This can be also extended to explain the preferable selection of tension twinning instead of basal slip in some grains and activation of non-basal slip like prismatic slip.

(7) Final twin variant types were mostly determined at the very early stages of compression dominated by basal slip. The subsequent increased stress further increased the twin number and facilitate the twin growth but did not change the tension twin variant selection behaviour. Non-basal slip played negligible role in the formation of tension twins and corresponding variant selection during entire compression test.

Acknowledgements

This work was funded by the EPSRC DARE Project, EP/L025213/1. The fruitful discussion with Prof. Zhang-Zhi Shi from University of Science and Technology Beijing is gratefully acknowledged.

References

[1] H. El Kadiri, C.D. Barrett, J. Wang, C.N. Tomé, Why are twins profuse in magnesium?, Acta Mater. 85 (2015) 354-361.
[2] M.R. Barnett, Twinning and the ductility of magnesium alloys: Part I: “Tension” twins, Mater. Sci. Eng. A 464 (2007) 1-7.
[3] L. Bao, C. Schuman, J.-S. Lecomte, M.-J. Philippe, X. Zhao, C. Esling, A Study of Twin Variant Selection and Twin Growth in Titanium, Adv. Eng. Mater. 13 (2011) 928-932.
[4] R. Xin, C. Guo, J.J. Jonas, G. Chen, Q. Liu, Variant selection of {10-12}-{10-12} double twins during the tensile deformation of an AZ31 Mg alloy, Mater. Sci. Eng. A 700 (2017) 226-233.
[5] S. Godet, L. Jiang, A.A. Luo, J.J. Jonas, Use of Schmid factors to select extension twin variants in extruded magnesium alloy tubes, Scr. Mater. 55 (2006) 1055-1058.
[6] I.J. Beyerlein, L. Capolungo, P.E. Marshall, R.J. McCabe, C.N. Tomé, Statistical analyses of deformation twinning in magnesium, Philos. Mag. 90 (2010) 2161-2190.
[7] J.J. Jonas, S. Mu, T. Al-Samman, G. Gottstein, L. Jiang, Ė. Martin, The role of strain accommodation during the variant selection of primary twins in magnesium, Acta Mater. 59 (2011) 2046-2056.
[8] S. Mu, J.J. Jonas, G. Gottstein, Variant selection of primary, secondary and tertiary twins in a deformed Mg alloy, Acta Mater. 60 (2012) 2043-2053.
[9] Z.-Z. Shi, Y. Zhang, F. Wagner, P.-A. Juan, S. Berbenni, L. Capolungo, J.-S. Lecomte, T. Richeton, On the selection of extension twin variants with low Schmid factors in a deformed Mg alloy, Acta Mater. 83 (2015) 17-28.
[10] M. Arul Kumar, I.J. Beyerlein, C.N. Tomé, A measure of plastic anisotropy for hexagonal close packed metals: Application to alloying effects on the formability of Mg, J. Alloys Compd. 695 (2017) 1488-1497.
[11] K.D. Molodov, T. Al-Samman, D.A. Molodov, Profuse slip transmission across twin boundaries in magnesium, Acta Mater. 124 (2017) 397-409.
[12] X. Liu, J.J. Jonas, B.W. Zhu, T. Wang, L.X. Li, Variant selection of primary extension twins in AZ31 magnesium deformed at 400°C, Mater. Sci. Eng. A 649 (2016) 461-467.
[13] M. Arul Kumar, I.J. Beyerlein, R.J. McCabe, C.N. Tomé, Grain neighbour effects on twin transmission in hexagonal close-packed materials, Nature Communications 7 (2016) 13826.
[14] G. Liu, R. Xin, X. Shu, C. Wang, Q. Liu, The mechanism of twinning activation and variant selection in magnesium alloys dominated by slip deformation, J. Alloys Compd. 687 (2016) 352-359.
[15] Z.-Z. Shi, Compound cross-grain boundary extension twin structure and its related twin variant selection in a deformed Mg alloy, J. Alloys Compd. 716 (2017) 128-136.
[16] F. Wang, S. Sandlöbes, M. Diehl, L. Sharma, F. Roters, D. Raabe, In situ observation of collective grain-scale mechanics in Mg and Mg–rare earth alloys, Acta Mater. 80 (2014) 77-93.
[17] Z.-Z. Shi, X.-F. Liu, Characteristics of cross grain boundary contraction twin pairs and bands in a deformed Mg alloy, J. Alloys Compd. 692 (2017) 274-279.
[18] L. Wang, Y. Yang, P. Eisenlohr, T.R. Bieler, M.A. Crimp, D.E. Mason, Twin Nucleation by Slip Transfer across Grain Boundaries in Commercial Purity Titanium, Metall. Mater. Trans. A 41 (2009) 421.
[19] J. Luster, M.A. Morris, Compatibility of deformation in two-phase Ti-Al alloys: Dependence on microstructure and orientation relationships, Metall. Mater. Trans. A 26 (1995) 1745-1756.
[20] T.R. Bieler, P. Eisenlohr, F. Roters, D. Kumar, D.E. Mason, M.A. Crimp, D. Raabe, The role of heterogeneous deformation on damage nucleation at grain boundaries in single phase metals, Int. J. Plast. 25 (2009) 1655-1683.
[21] J.L. Li, D. Wu, R.S. Chen, E.H. Han, Anomalous effects of strain rate on the room-temperature ductility of a cast Mg-Gd-Y-Zr alloy, Acta Mater. 159 (2018) 31-45.

[22] A. Khosravani, D.T. Fullwood, B.L. Adams, T.M. Rampton, M.P. Miles, R.K. Mishra, Nucleation and propagation of twins in AZ31 magnesium alloy, Acta Mater. 100 (2015) 202-214.
[23] Y. Guo, T.B. Britton, A.J. Wilkinson, Slip band–grain boundary interactions in commercial-purity titanium, Acta Mater. 76 (2014) 1-12.
[24] J. Zhang, G. Xi, X. Wan, C. Fang, The dislocation-twin interaction and evolution of twin boundary in AZ31 Mg alloy, Acta Mater. 133 (2017) 208-216.
[25] D. Guan, W.M. Rainforth, J. Gao, J. Sharp, B. Wynne, L. Ma, Individual effect of recrystallisation nucleation sites on texture weakening in a magnesium alloy: Part 1- double twins, Acta Mater. 135 (2017) 14-24.
[26] F. Bachmann, R. Hielscher, H. Schaeben, Texture Analysis with MTEX – Free and Open Source Software Toolbox, Solid State Phenomena 160 (2010) 63-68.
[27] S.R. Agnew, R.P. Mulay, F.J. Polesak, C.A. Calhoun, J.J. Bhattacharyya, B. Clausen, In situ neutron diffraction and polycrystal plasticity modeling of a Mg–Y–Nd–Zr alloy: Effects of precipitation on individual deformation mechanisms, Acta Mater. 61 (2013) 3769-3780.
[28] P. Crawforth, Towards a Micromechanistic Understanding of Imparted Subsurface Deformation During Machining of Titanium Alloys, University of Sheffield, 2014.
[29] S. Xu, L.S. Toth, C. Schuman, J.-S. Lecomte, M.R. Barnett, Dislocation mediated variant selection for secondary twinning in compression of pure titanium, Acta Mater. 124 (2017) 59-70.
[30] B.L. Wu, G.S. Duan, X.H. Du, L.H. Song, Y.D. Zhang, M.J. Philippe, C. Esling, In situ investigation of extension twinning-detwinning and its effect on the mechanical behavior of AZ31B magnesium alloy, Materials & Design 132 (2017) 57-65.
[31] D. Drozdenko, J. Bohlen, S. Yi, P. Minárik, F. Chmelík, P. Dobroň, Investigating a twinning–detwinning process in wrought Mg alloys by the acoustic emission technique, Acta Mater. 110 (2016) 103-113.
[32] Z.-Z. Shi, Secondary twin variant selection in Mg alloy after a strain-path change, J. Alloys Compd. 696 (2017) 510-515.

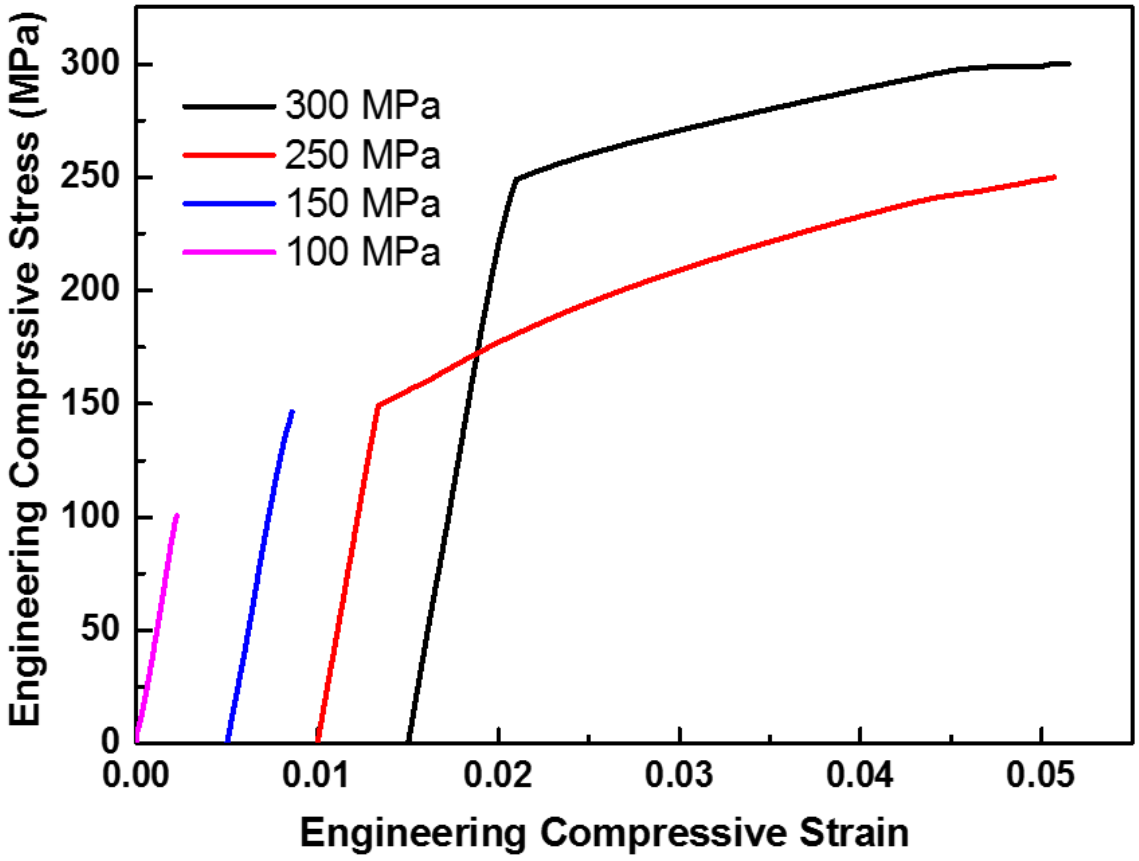

Fig.1 Interrupted compression strain-stress curves with a strain rate of 10^{-1} s^{-1}.

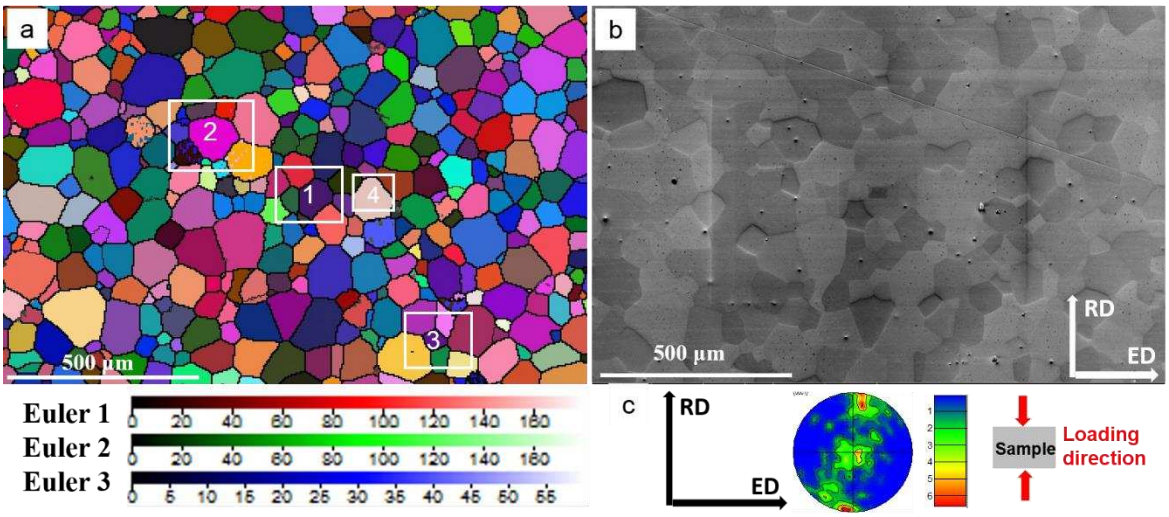

Fig.2 (a) EBSD all Euler image and (b) corresponding SEM image of the sample before compression, (c) (0002) pole figure of (a).

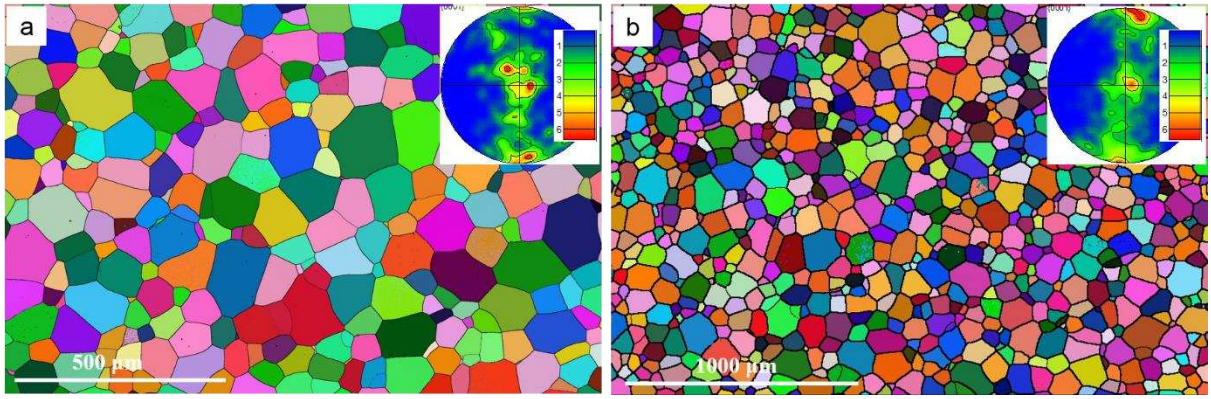

Fig.3 EBSD all Euler images of (a) another sample having the same sampling area as sample in Fig. 2(a), and (b) another sample having four times sampling area as sample in Fig. 2(a). The insets are the corresponding (0002) pole figures.

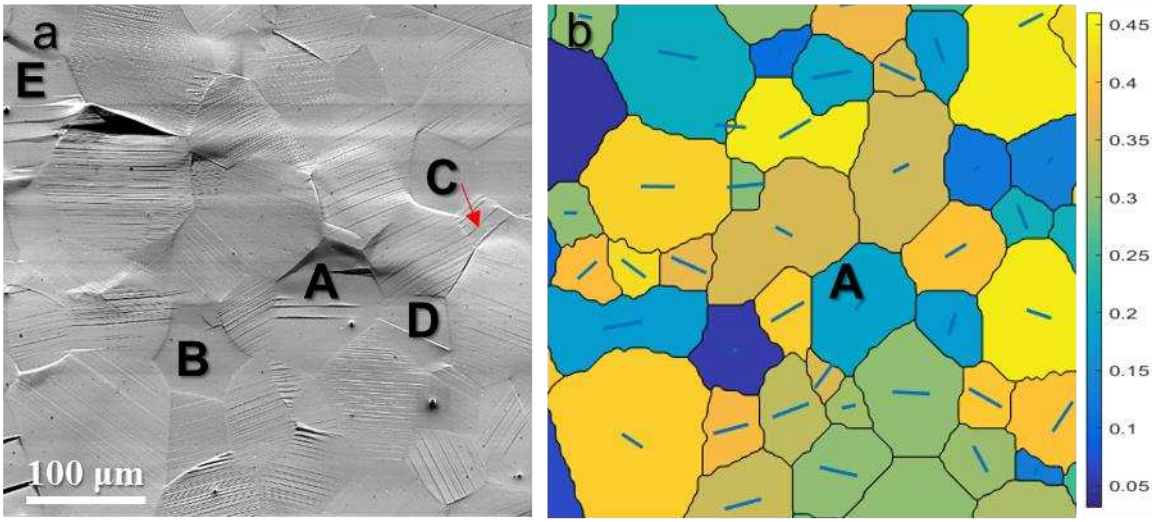

Fig. 4 (a) a typical SEM image of the sample surface after compression at 100 MPa, and (b) predicted basal slip traces and basal slip macro Schmidt Factor distribution.

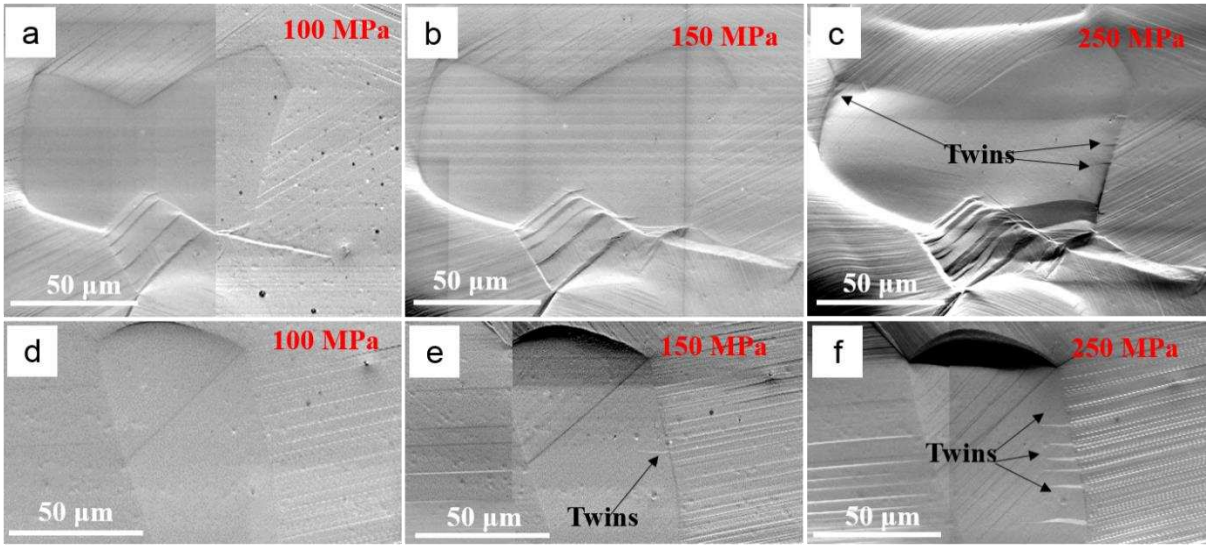

Fig. 5 Typical SEM image of a sample surface after compression at (a) 100 MPa, (b) 150 MPa, and (c) 250 MPa; another sample surface after compression at (d) 100 MPa, (e) 150 MPa, and (f) 250 MPa.

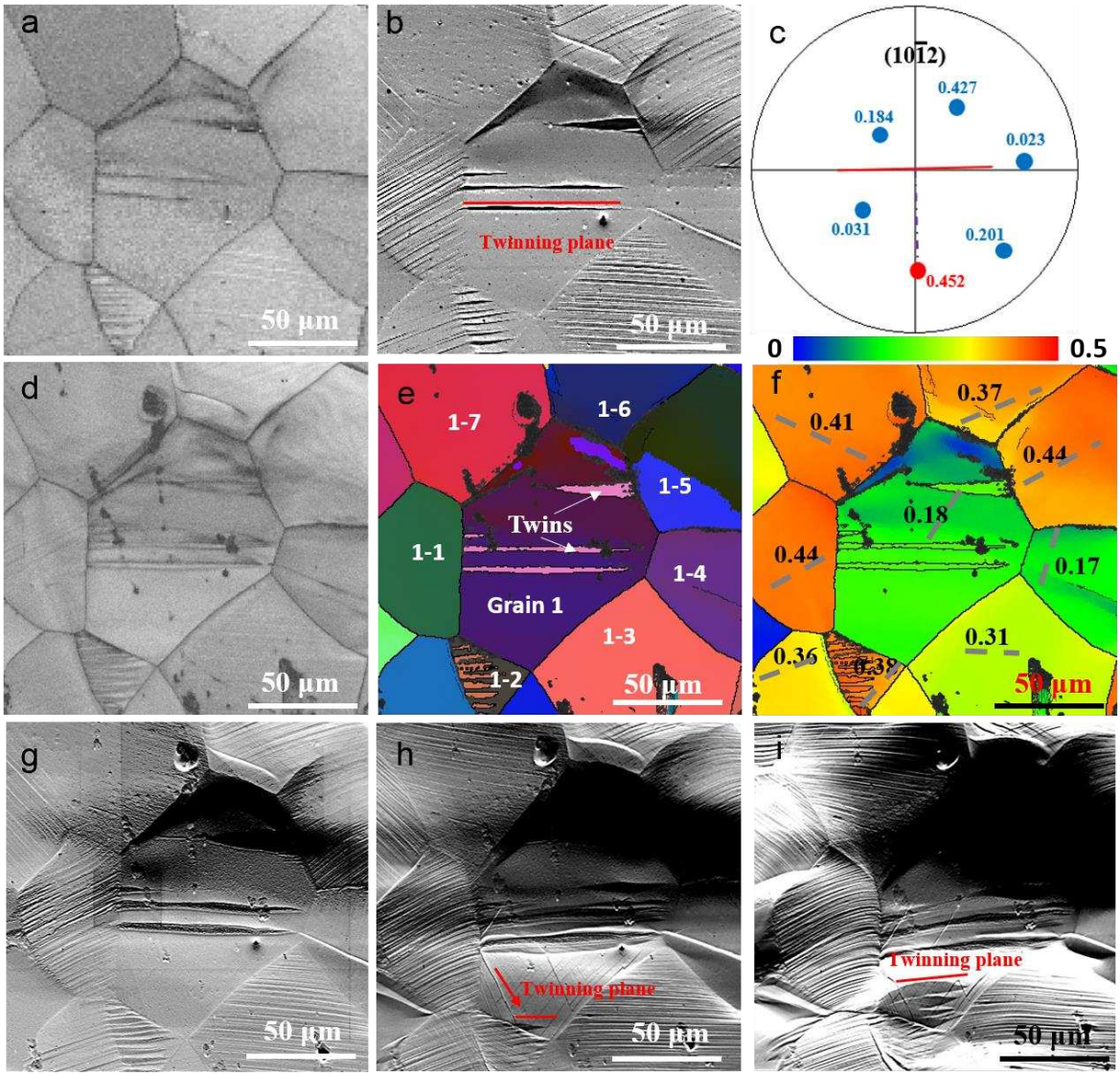

Fig. 6 (a) EBSD band contrast and (b) corresponding SEM images of region of interest 1 after being compressed at the stress of 100 MPa. (c) (10$\bar{1}$2) pole figure of grain 1. (d) EBSD band contrast and (e) All Euler and (f) MSF distribution images of region of interest 1 after being compressed at the stress of 150 MPa. (g-i) corresponding SEM images of sample compressed at the stress of 150, 250 and 300 MPa.

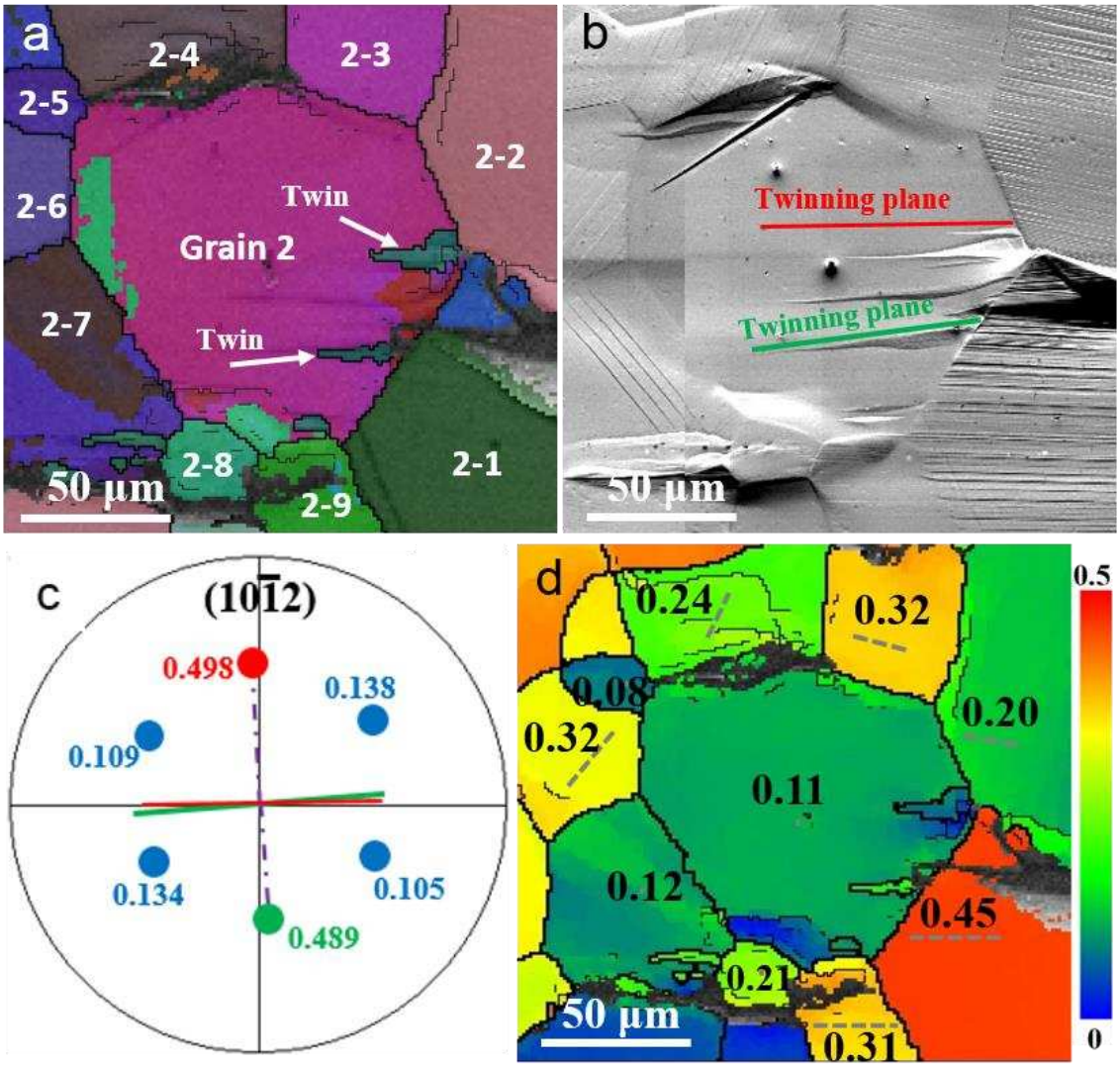

Fig. 7 (a) EBSD all Euler and (b) corresponding SEM images of region of interest 2 after being compressed at the stress of 100 MPa. (c) $(10\bar{1}2)$ pole figure of grain 2. (d) EBSD MSF distribution superimposed with basal slip traces.

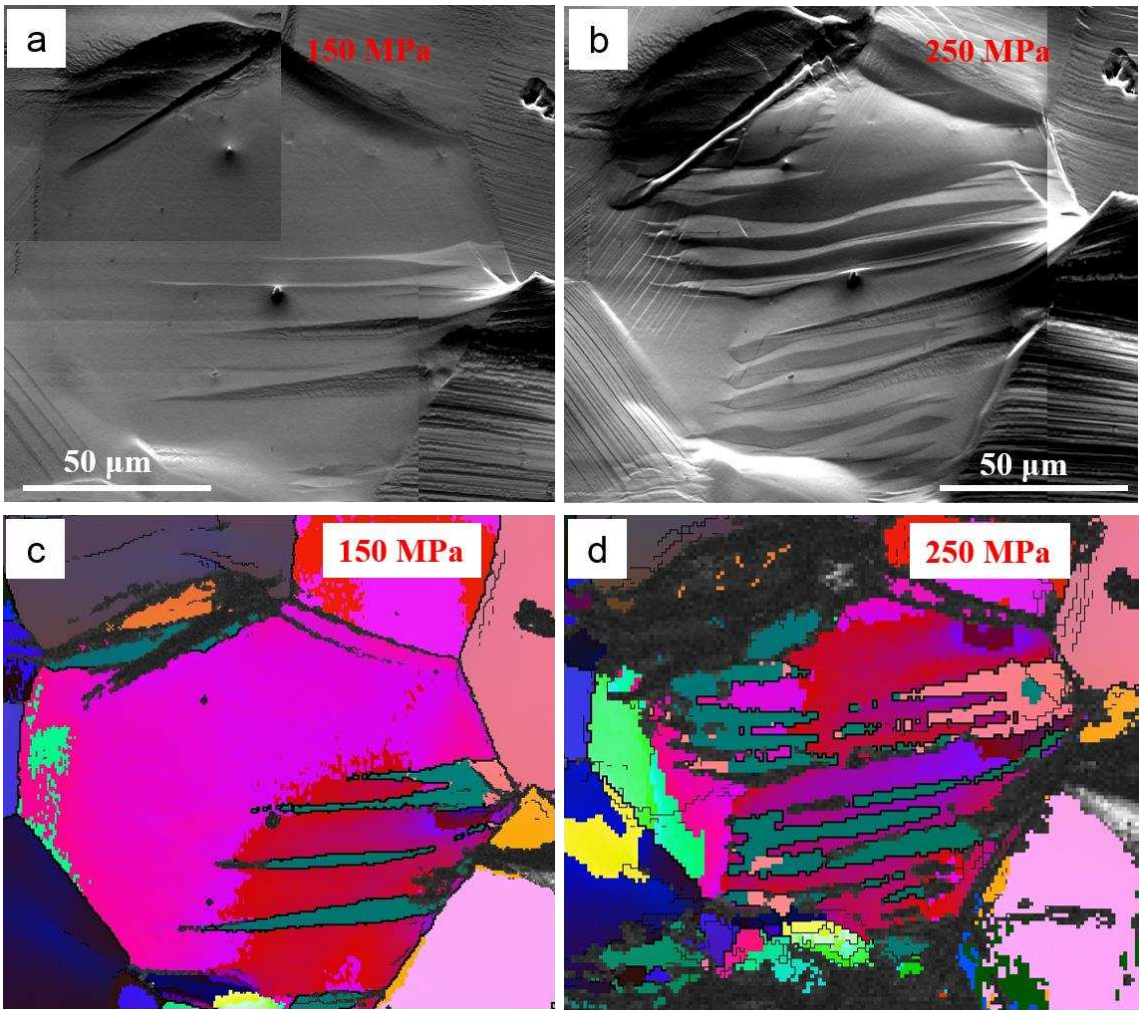

Fig. 8 SEM images of Grain 2 after being compressed at stress of (a) 150 MPa and (b) 250 MPa; corresponding EBSD all Euler images of (c) 150 MPa and (d) 250 MPa.

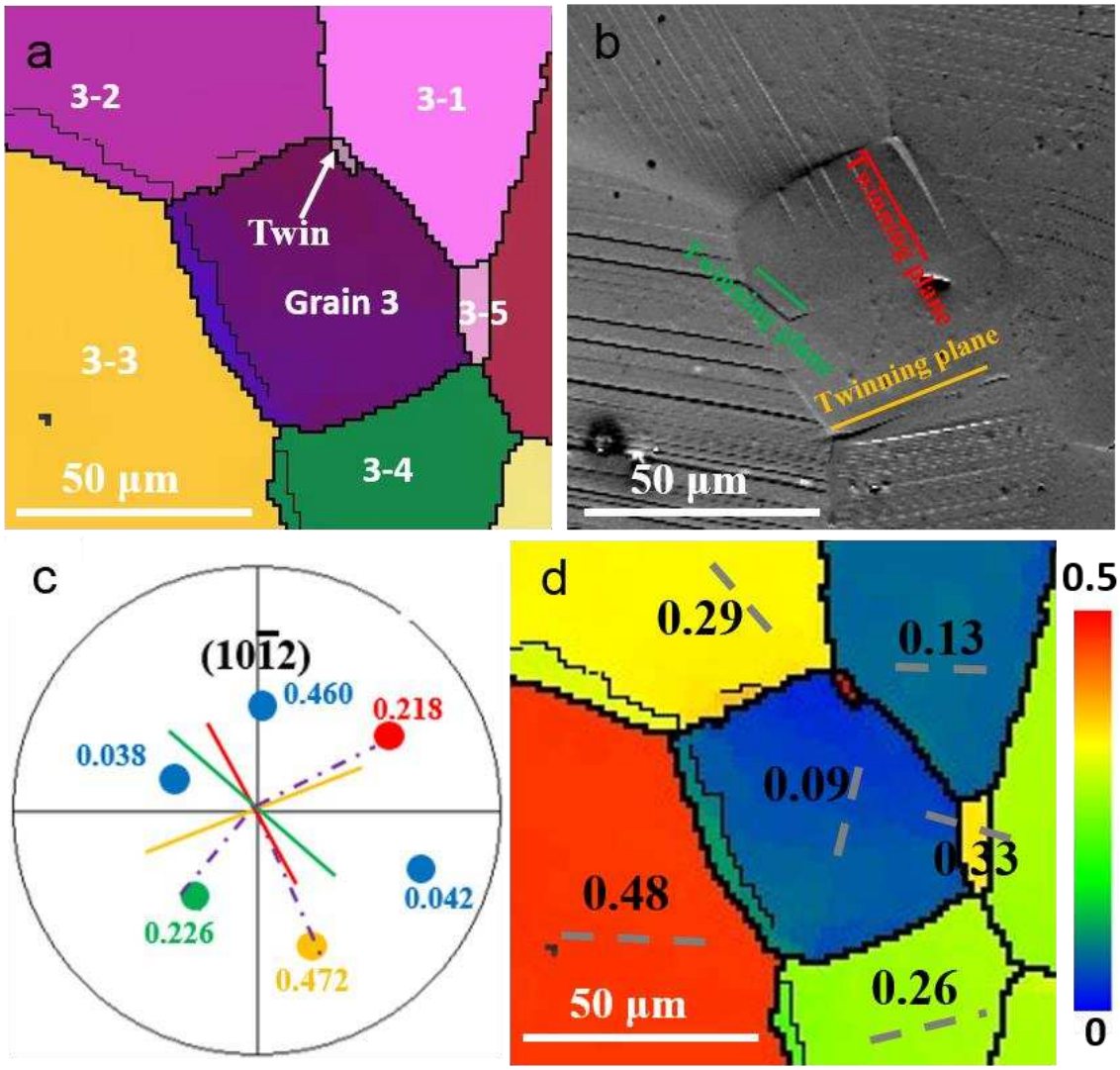

Fig. 9 (a) EBSD all Euler and (b) corresponding SEM images of region of interest 3 after being compressed at the stress of 100 MPa. (c) $(10\bar{1}2)$ pole figure of grain 3. (d) EBSD MSF distribution superimposed with basal slip traces.

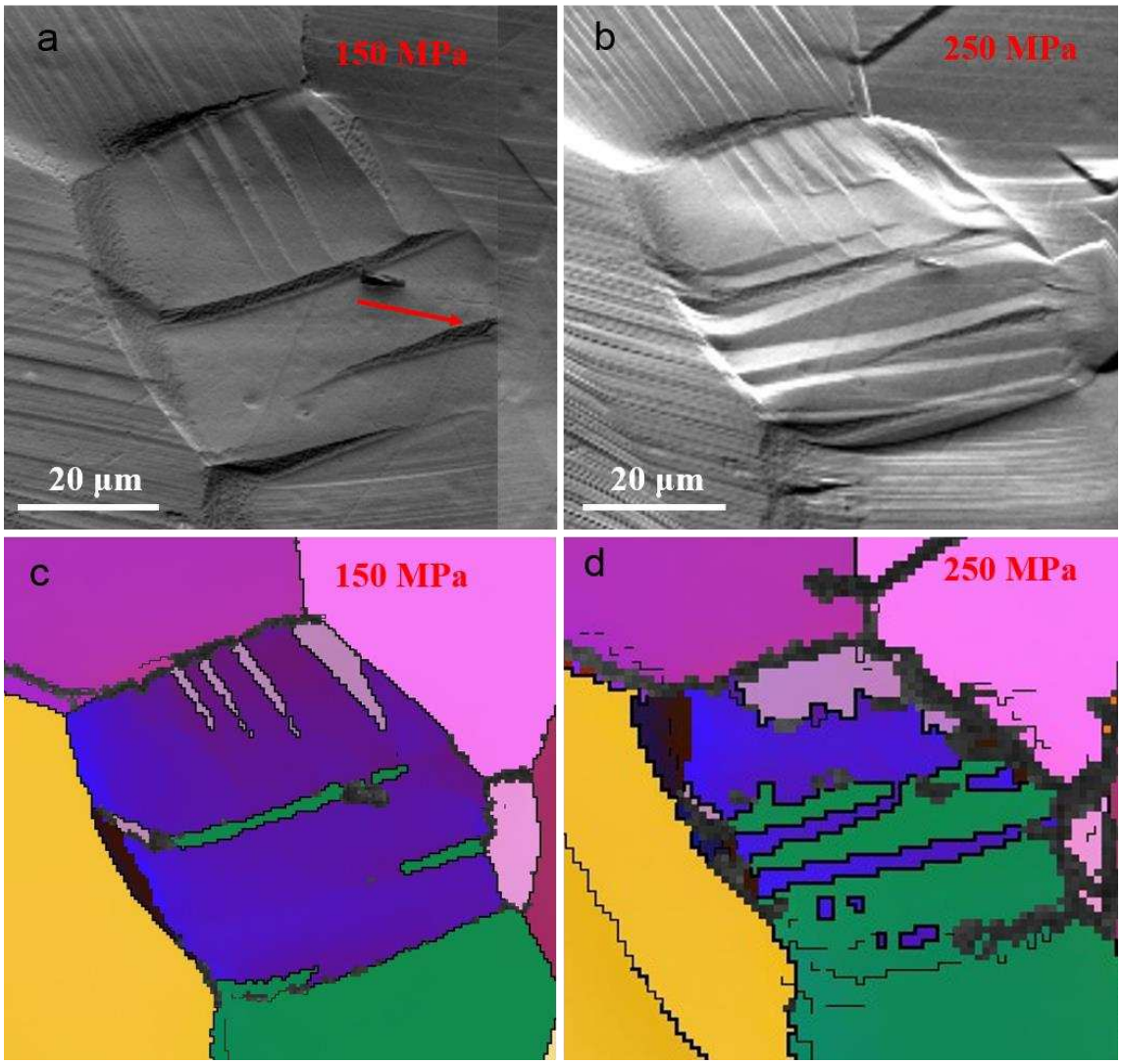

Fig. 10 SEM images of Grain 3 after being compressed at stress of (a) 150 MPa and (b) 250 MPa; corresponding EBSD all Euler images of (c) 150 MPa and (d) 250 MPa.

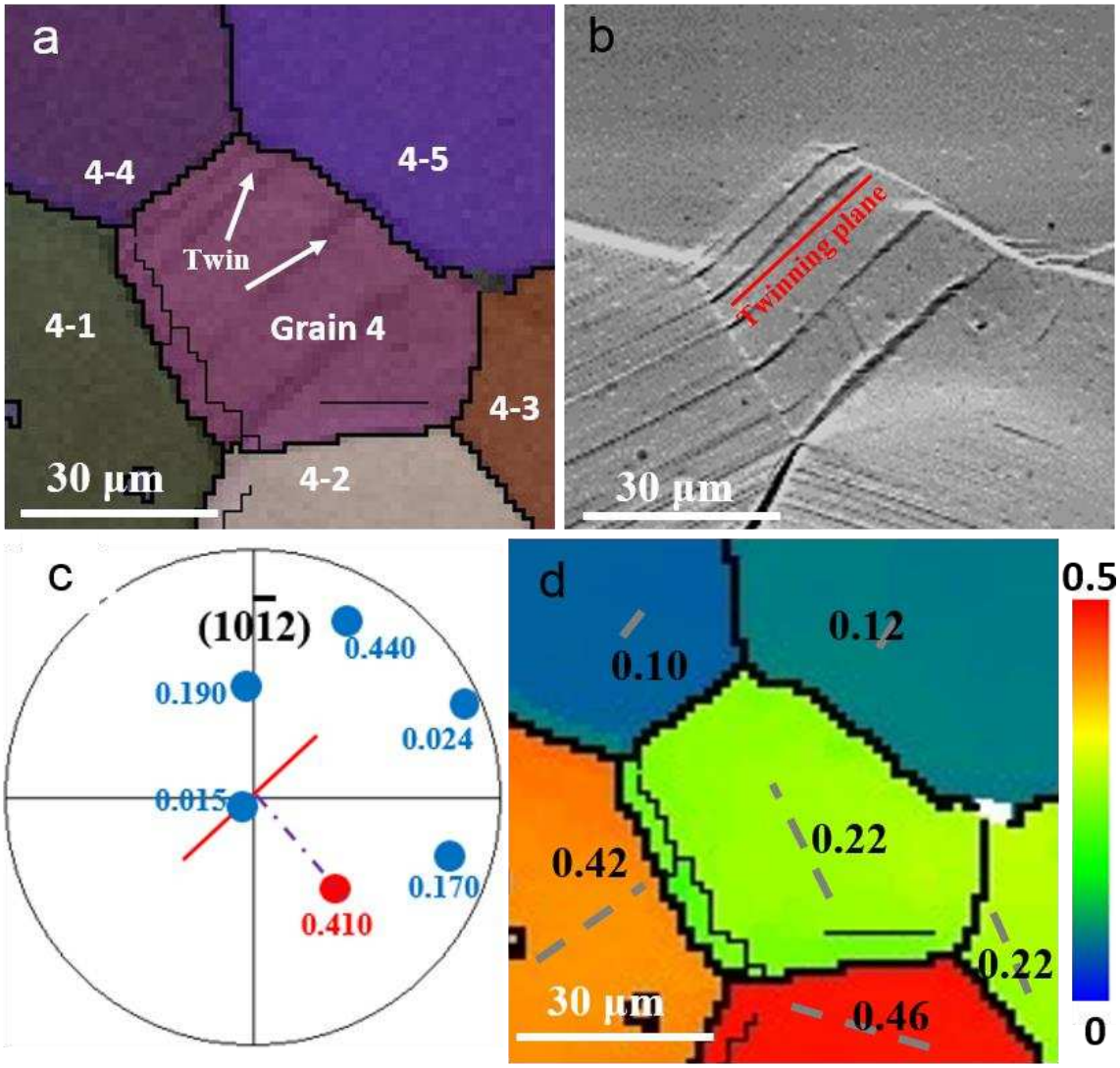

Fig. 11 (a) EBSD all Euler and (b) corresponding SEM images of region of interest 4 after being compressed at the stress of 100 MPa. (c) (10$\bar{1}$2) pole figure of grain 4. (d) EBSD MSF distribution superimposed with basal slip traces.

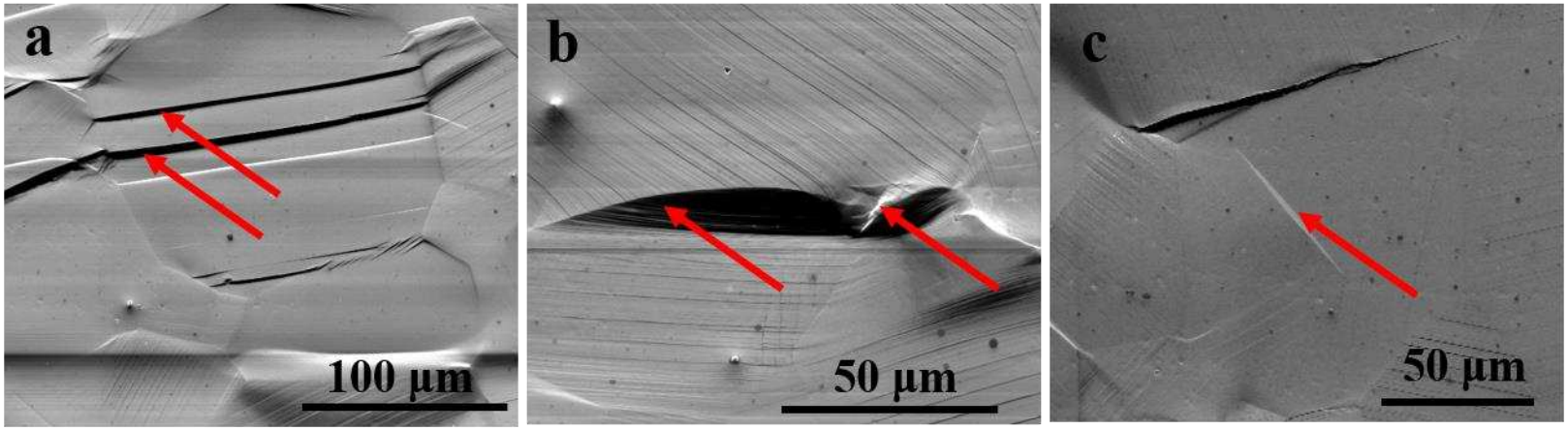

Fig. 12 SEM images of (a) kink bands, (b) bulging grain boundaries, and (c) tension twins without connecting to grain boudaries after being compressed to 100 MPa.

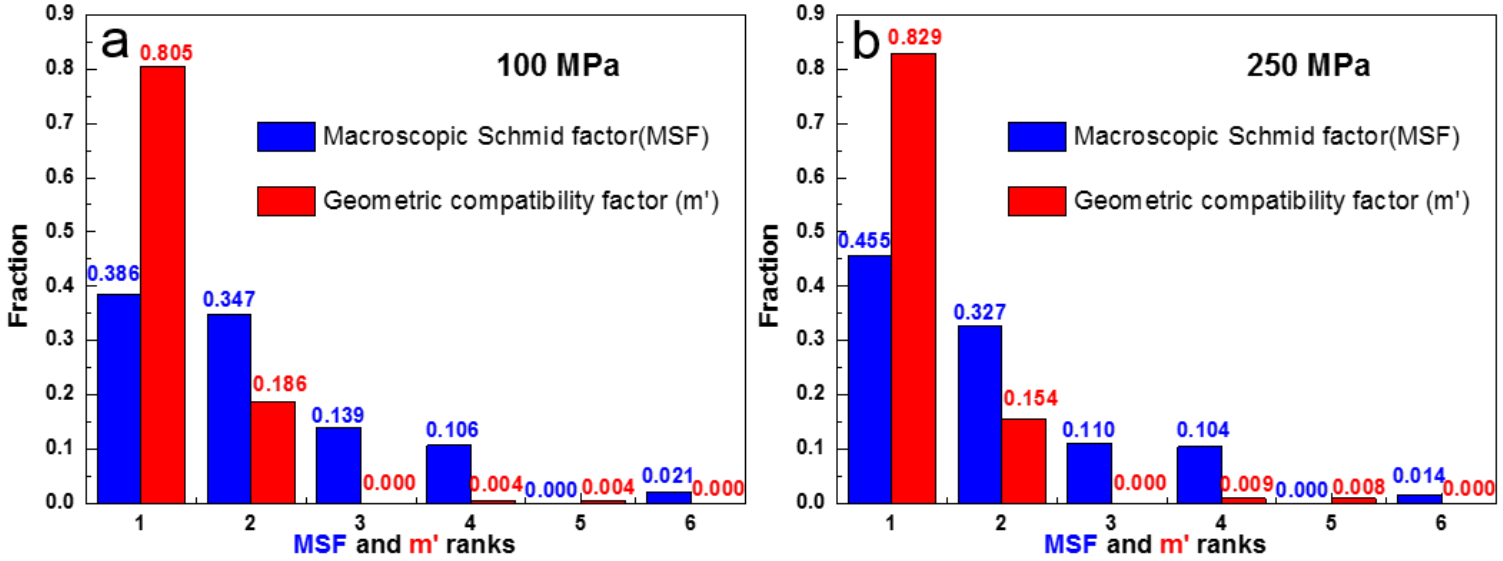

Fig. 13 MSF(m)-m' ranking and proportions after being compressed to (a) 100 MPa and (b) 250 MPa.

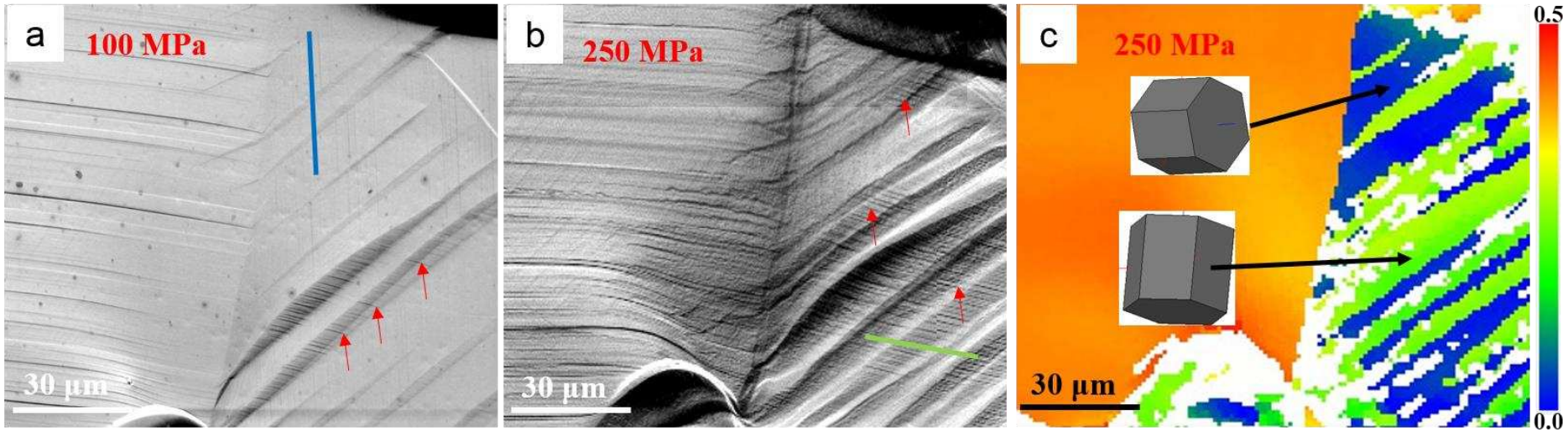

Fig. 14 (a-b) SEM images of a typical de-twinning region after being compressed to 100 MPa and 250 MPa, (c) EBSD map of basal slip MSF distribution after being compressed to 250 MPa. Blue and green lines indicate basal slip plane traces of matrix and twins, respectively. The basal slip traces of twins were out of twin boundaries after de-twinning during unloading, marked by red arrows.

Table 1 m' between basal slip or twinning of neighbouring grains and 6 tension twin variants in Grain 1 tabulated with the MSF for each twin variant

Neighbouring grain	MSF of 6 tension twin variants in Grain 1					
	0.452 m'	0.427 m'	0.201 m'	0.184 m'	0.031 m'	0.023 m'
1-1	**0.826**[a]	0.003	0.570	0.041	0.253	0.041
1-2(twin)	**0.884**[b]	0.004	0.304	0.022	0.563	0.012
1-3	0.323	0.573	0.187	0.472	0.059	0.178
1-4	N/A	N/A	N/A	N/A	N/A	N/A
1-5	**0.778**[a]	0.226	0.344	0.003	0.452	0.204
1-6	0.741	0.313	0.447	0.161	0.349	0.097
1-7	0.008	0.486	0.112	0.809	0.329	0.114

[a] activated twining variant red highlighted in Fig. 6(b-c)

[b] activated twining variant red highlighted in Fig. 6(h-i)

Table 2 m' between basal slip or twinning of neighbouring grains and 6 tension twin variants in Grain 2 tabulated with the MSF for each twin variant

Neighbour grain	MSF of 6 tension twin variants in Grain 2					
	0.498	0.489	0.138	0.134	0.109	0.105
	m'	m'	m'	m'	m'	m'
2-1	0.073	**0.888**[c]	0.001	0.520	0.028	0.471
2-2	**0.614**[d]	0.171	0.198	0.229	0.351	0.006
2-3	0.323	0.573	0.187	0.472	0.059	0.178
2-4	0.163	0.438	0.511	0.174	0.000	0.084
2-5	N/A	N/A	N/A	N/A	N/A	N/A
2-6	0.093	0.708	0.253	0.310	0.011	0.249
2-7	N/A	N/A	N/A	N/A	N/A	N/A
2-8	N/A	N/A	N/A	N/A	N/A	N/A
2-9	N/A	N/A	N/A	N/A	N/A	N/A

[c] activated twining variant green highlighted in Fig. 7(b-c)

[d] activated twining variant red highlighted in Fig. 7(b-c)

Table 3 m' between basal slip or twinning of neighbouring grains and 6 tension twin variants in Grain 3 tabulated with the MSF for each twin variant

Neighbour grain	MSF of 6 tension twin variants in Grain 3					
	0.472	0.460	0.226	0.218	0.042	0.038
	m'	m'	m'	m'	m'	m'
3-1	0.216	0.438	0.406	0.087	0.001	0.160
3-2	0.108	0.783	0.073	**0.816**[e]	0.197	0.200
3-3	**0.867**[f]	0.031	**0.843**[g]	0.015	0.255	0.215
3-4	0.008	0.016	0.195	0.224	0.211	0.232
3-5	0.712	0.098	0.516	0.199	0.175	0.079

[e] activated twining variant red highlighted in Fig. 9(b-c)

[f] activated twining variant yellow highlighted in Fig. 9(b-c)

[g] activated twining variant green highlighted in Fig. 9(b-c)

Table 4 m' between basal slip or twinning of neighbouring grains and 6 tension twin variants in Grain 4 tabulated with the MSF for each twin variant

Neighbour grain	MSF of 6 tension twin variants in Grain 4					
	0.440	0.410	0.190	0.170	0.024	0.015
	m'	m'	m'	m'	m'	m'
4-1	0.001	**0.987**[h]	0.088	0.488	0.041	0.628
4-2	0.017	0.656	0.019	0.208	0.205	0.241
4-3	0.524	0.538	0.291	0.308	0.230	0.233
4-4	N/A	N/A	N/A	N/A	N/A	N/A
4-5	N/A	N/A	N/A	N/A	N/A	N/A

[h] activated twining variant red highlighted in Fig. 11(b-c)